Biomass and Bioenergy 208 (2026) 108879

Contents lists available at ScienceDirect

Biomass and Bioenergy

journal homepage: www.elsevier.com/locate/biombioe

Sustainable synthesis of energy-dense hydrochar from food waste blends via hydrothermal carbonisation: Process optimisation and characterisation using response surface methodology

Danai Pasipanodya [a], Naadhira Seedat [b,*], Bilal Patel [c], Rishen Roopchund [d]

[a] Department of Chemical Engineering, Doornfontein Campus, University of Johannesburg, Johannesburg, 2094, South Africa
[b] Department of Chemical Engineering, Faculty of Engineering, the Built Environment and Information Technology, University of Pretoria, 0028, South Africa
[c] Institute for Catalysis and Energy Solutions (ICES), University of South Africa, UNISA Science Campus, Florida, Johannesburg, 1709, South Africa
[d] Department of Chemical and Materials Engineering, College of Science, Engineering and Technology, University of South Africa, Roodepoort, 1709, South Africa

ARTICLE INFO

Keywords:
Central composite design
Food waste
Hydrochar
Hydrothermal carbonisation
Optimisation
Response surface methodology

ABSTRACT

Hydrothermal carbonisation (HTC) was used to convert food waste (FW), comprising butternut waste (BW) and potato peels (PP), into hydrochar (HC). A central composite design (CCD) with response surface methodology (RSM) was used to investigate the effects of HTC temperature (140–300 °C), residence time (22–248 min), solid-to-liquid (S/L) ratio (1:11–1:15), and BW/PP ratio on HC yield, surface area (SA), and higher heating value (HHV). The quadratic model well-described the yield, SA, and HHV responses. The RSM-CCD maximum yield (40.22 %), SA (7.86 m2/g), and HHV (29.351 MJ/kg) was achieved at temperature of 204 °C, residence time of 131.39 min, S/L ratio of 1:12.89, and BW/PP ratio (0.5:0.5). The predicted responses were closer to experimental runs, proving good model reproducibility. Notably, temperature had the most significant influence on SA and HHV, except for yield, which depends greatly on the FW ratio. This is because at higher temperatures, volatiles are more effectively driven off, concentrating the carbon-rich components that enhance both SA and HHV. At the same time, the yield is more dependent upon the FW ratio due to variations in feedstock composition. Elemental analysis showed lower H/C and O/C ratios at elevated temperatures, indicating improved carbonisation typically leads to a higher HHV and improved fuel quality. SEM and FTIR confirmed the flask-like structures and functional groups, which can play a significant role in the adsorption capabilities of HC for pollutant removal. The valorisation of FW into adsorbents and biofuels represents a dual breakthrough, transforming waste management practices while simultaneously reducing greenhouse gas emissions.

1. Introduction

Worldwide, the surge in population and rapid industrialisation has led to a significant increase in the generation of organic waste, particularly food waste (FW) [1]. According to the Food and Agriculture Organisation (FAO), FW contributes to about 1.6 billion tonnes of waste generated annually, where about 13 % of food production is lost between harvesting and retail stages and an additional 17 % discarded at consumption levels [2]. In the South African context, about 10 million tonnes of FW are discarded annually, equivalent to one-third of its total food production of 31 million tonnes [2]. Butternut waste (BW) and potato peels (PP) constitute a notable share of this FW stream. Nevertheless, these BW and PP residues remain largely untreated, overlooking the opportunity to convert them into a high-value product. FW essentially ends up in landfills and subsequently degrades, releasing potent greenhouse gases (GHGs) like methane (CH_4), which is 25 times more potent than CO_2 in terms of climate-forcing potential over a 100-year time period [3]. In addition, the incineration of FW residuals often produces a considerable amount of CO_2 emissions, exacerbating the existing atmospheric burden of GHGs and contributing further to climate change. Efforts to mitigate landfill-derived GHG emissions have been further underscored by the pledge of more than 100 nations to reduce CH_4 emissions by 30 % based on Vision 2030 goals [4].

Despite the challenges posed, the composition of FW makes it a potential source of value-added products [5]. The valorisation of FW has been investigated through various treatment methods, including anaerobic digestion, composting, animal feed, and thermochemical processes [6]. These treatment methods have advantages and

* Corresponding author.
E-mail address: naadhira.seedat@up.ac.za (N. Seedat).

https://doi.org/10.1016/j.biombioe.2025.108879
Received 16 October 2025; Received in revised form 18 December 2025; Accepted 18 December 2025
Available online 22 December 2025

limitations; nevertheless, research in FW treatment has focused on creating methane through anaerobic digestion [6]. Thermochemical processes such as pyrolysis and gasification have received less attention for treating food waste, possibly due to its high moisture content (>60 %) [7]. Thermochemical methods require waste to be relatively dry. An energy-intensive drying procedure is required to process high moisture content (MC) waste such as FW. Consequently, thermochemical recycling of FW remains one of the most underexplored approaches in the waste-to-energy field [6].

This necessitates the need to explore alternatives, such as hydrothermal carbonisation (HTC), which offers several advantages over other thermochemical conversion processes, including the handling of wet biomass, operating at moderate temperatures (<300 °C), and yielding hydrocarbons with higher energy density [6]. HTC typically involves treating wet biomass at moderate temperatures under self-generated pressure in an aqueous environment, yielding a carbon-dense solid product referred to as hydrochar (HC), with characteristics similar to those of lignite coal [8]. HTC involves a series of sequential reactions, mainly dehydration, hydrolysis, condensation, and decarboxylation [9,10]. The process yields three distinct products: HC, a small quantity of gaseous CO_2, and a nutrient and sugar-rich aqueous phase referred to as process water [11]. The HC product is characterised by its porous structure, elevated carbon content, and distinct surface functionalities, making it excellent for several industrial applications [11].

Recently, HTC has gained enormous attention as a novel approach to convert wet biomass into HC with wide potential applications such as soil conditioning and carbon sequestration [12], CO_2 capture [13], adsorption [14], energy storage devices and catalyst support [15]. The yield and quantity of HC through HTC are usually influenced by the type of feedstocks, time, and temperature, making the process complex, costly, and difficult to model and optimise using one-factor-at-a-time (OFAT) analysis. Optimising HTC through response surface methodology (RSM) rather than OFAT is crucial for maximising HC production with a higher heating value (HHV) and energy yield, thereby enabling scalable process development by analysing multi-parameter effects [16]. RSM allows for efficient optimisation by analysing multiple parameters and their interactions in fewer experimental runs, thereby identifying optimal conditions, making the process more efficient, cost-effective, and less time-consuming [17]. In particular, central composite design (CCD)-RSM usually provides superior predictive accuracy and interaction analysis across the design space compared to Box-Behnken design and optimal (custom) designs [18].

Most previous studies have explored HTC for singular feedstocks as precursors for HC, including cornstalk Kang et al. [19], rice husk Zulkornain et al. [20], and oat husk Murillo et al. [21]. However, research on HTC of mixed feedstocks, such as BW and PP, which can potentially enhance HC properties through synergistic effects, remains limited. Furthermore, the crucial aspect of the trade-off between optimising yield, HHV, and surface area (SA) remains under-researched, despite its importance for practical applications in energy and adsorption. The characteristics of HC materials, such as SA and HHV, are key factors that directly govern the pollutant adsorption capacity and energy density, respectively. The optimisation of yield and key characteristics (SA and HHV) of HC materials are crucial, as they respectively determine the economic output and directly govern performance in pollutant adsorption and energy applications. Therefore, the present study aims to address these gaps by employing CCD-RSM to evaluate the combined effects of temperature, reaction time, solid-to-liquid ratio, and feedstock composition on HC yield, HHV, and SA response. By integrating these variables, this research presents a multi-response optimisation strategy that enhances our understanding of HC properties and offers comprehensive insights for developing tailored HC with improved functional properties for sustainable applications for energy and adsorption purposes.

2. Materials and methods

2.1. Materials and sample preparation

The FW utilised in this study comprised BW and PP. The BW was obtained from Joburg Market City Deep dumpsters, South Africa's major centre for marketing fresh produce. The PP wastes were collected from the Sebhuku fast food restaurant in Doornfontein, Johannesburg. The FW was then separately blended into smaller uniform particles (2–4 mm) to promote homogeneity and better mixing inside the reactor. The blended FW was stored in a refrigerator at 4 °C at the University of Johannesburg, Doornfontein campus, to preserve its moisture and prevent degradation before the HTC experiment.

2.2. Chemicals used

De-ionised water supplied by Laboratory Supplies was used as a solvent and reaction medium for the HTC process. Nitrogen gas (N_2) with 99.9 % purity, supplied by Afrox Ltd (SA), was used to purge oxygen from inside the reactor, making the environment inert before the start of the experiment.

2.3. HTC experimental setup procedure

HTC tests were carried out in a batch system, and each test was carried out in a desktop stainless steel high-pressure reactor with a total capacity of 1000 mL and a working volume of 800 mL. The reactor was equipped with a mechanical stirrer to ensure uniform mixing of the feedstock and to promote effective heat transfer during the reaction. Before each experimental run, the pressure vessel and the magnetic stirrer were thoroughly cleaned with soap and de-ionised to remove impurities. The BW and PP were weighed using a scale and added to the reactor vessel to start the experiment. For each run, 50g of either BW or PP on a dry basis was added to the reactor. The inherent moisture content (MC) in the wet feedstock was incorporated into the total liquid mass for the reaction. Due to the difference in MC of the PP and the BW, the wet basis mass of the two feedstocks differed. To obtain 50g of dry basis mass of PP with a MC of 78 %, 227g of moist PP were weighed. Similarly, 417g of moist BW with a MC of 88 % was weighed to obtain 50g on a dry basis. To get 50g dry basis mass for the runs with a 50 % mix of the FW samples, 113.5g of PP and 208.5g of BW were weighed. After loading the FW into the reactor, de-ionised water was added based on the solid-liquid ratio (S/L ratio). Before the experimental run, N_2 was used to eliminate all the oxygen inside the reactor. To purge the system, the gas valves of the reactor were opened, allowing nitrogen from the connected cylinder to flow in and out for 3 min. Afterwards, the gas valves were closed. The magnetic stirrer was turned on and set to 100 rpm. The vessel was heated to the desired temperature at a constant heating rate of 5 °C/min using a heating jacket, and the temperature was sustained within ±10 °C of the set point throughout the experiment duration. Upon completion of each run, the reactor was left to cool overnight. Non-condensable gases such as CO_2, CO, H_2O vapour, and CH_4 were vented through a fume hood. The HC and liquid products were then separated via vacuum filtration. The resulting wet HC was dried in a hot air oven at 105 °C for 24 h. Once thoroughly dried, the HC was collected and stored in sealed plastic sample bags for subsequent analysis. Equation (1) was used to calculate the HC mass yield on a dry basis [22].

$$\%\ \text{Yield} = \frac{\text{Mass of dry HC}}{\text{Mass of dry feedstock}} \times 100\% \quad (1)$$

2.4. Characterisation of food waste and hydrochar samples

2.4.1. Crystallographic, functional groups, textural properties, surface morphology, and thermogravimetric analysis

X-ray Diffraction (XRD, Siemens D 501 model) with Ni-filtered CuKα radiation (α = 1.54056 Å) set at 2Theta (2θ) range (10°–90°) was used to determine the crystalline and amorphous structure of the FW and HC samples. Fourier transform infrared spectroscopy (FTIR, Thermo Scientific spectrometer) set at wavenumber the 400 to 4000 cm^{-1} spectral range was used to identify the functional groups of HC and BW samples. Micrometrics TriStar II using Brunauer-Emmett-Teller (BET) method was used to determine the SA measured via N_2 adsorption after samples (BW and HC) degassing at 120 °C. The Scanning Electron Microscope (SEM, JOEL JSM-7900 F model) operated with an emission current of 61.6 μA, magnification of ×2000–x10000, and a working distance of 10 mm was used to examine surface morphology of the samples. A thermogravimetric analyser (TGA, HITACHI STA-7200RV model) was used evaluate the thermal decomposition of the FW and HC samples at a temperature range of 25–1000 °C (heating rate of 20 °C/min under) inert environment with a nitrogen flow rate of 25 mL/min.

2.4.2. Ultimate analysis, proximate analysis and higher heating value

LECO TruSpec analyser following ISO 12902 and ISO 19579-CHNS instrumental method was used to determine the ultimate analysis, particularly quantifying the elemental composition (carbon (C), hydrogen (H), nitrogen (N), oxygen (O), and sulphur (S) content). Oxygen content was estimated using Equation (2).

$$\text{Oxygen \%} = 100 - (\text{Carbon \%} + \text{Hydrogen \%} + \text{Nitrogen \%} + \text{Sulphur \%} + \text{Ash\%}) \quad (2)$$

Proximate analysis of FW and HC samples were conducted following the Automated thermogravimetry (ASTM D5142) standard to determine volatile matter (VM), MC, fixed carbon (FC), and ash content using LECO TGA 701 instrument. Briefly, MC, VM, and ash content measured via thermogravimetric analysis at set temperatures of 107 °C in an inert atmosphere and isothermally, continue heating the same sample under nitrogen to 950 °C, and purging oxygen gas at 950 °C and hold to combust all carbon, respectively. The remaining non-combustible residue was recorded as Ash %. FC was computed by subtracting the sum of other components (MC, VM, and Ash %) from the total mass. HHV of FW and HC samples were measured using Leconfield bomb calorimeter calibrated with benzoic acid.

2.5. Experimental design

The HTC experimental runs were designed and optimised using CCD-RSM method using Design Expert 13 software. CCD was used because of it can fit full quadratic models, efficiently explore factor interaction and evaluate non-linear relationship, robust predictive power, and build on factorial designs. Four parameters mainly A-temperature (140–300 °C), B-residence time (22–248 min), C-S/L ratio (1:11–1:15) including the moisture present in feedstock, and D-BW/PP ratio. Note, numerical values (0, 0.5, and 1) were used to represent the BW, mixed BW/PP (1:1), and PP, respectively, because the CCD framework requires quantitative rather than categorical inputs. The parameter value ranges were based on related studies [23]; [24]; [25]. To enhance model reliability and predictive accuracy, 30 experimental runs were performed Supplementary Information Table S1. The design structure included a mix of factorial, axial, and centre points in a ratio of 16:8:6. Additionally, Analysis of Variance (ANOVA) was also employed to assess statistical validity. In RSM, ANOVA statistical indicators including sequential p-value (<0.05), lack of fit p-value (>0.05), coefficient of regression (R^2), and coefficient of variance (C.V.% ≤ 10) were used to confirm the significance of higher-order terms, verify model adequacy, indicate explained variance, and check reproducibility of the model, respectively [26].

3. Results and discussion

3.1. HTC modelling and ANOVA analysis

Table S2 depicts the model fit summary based on statistical metrics of the three response factors (mass yield, SA, and HHV). The interpretation of the statistical metrics is well-explained by Orero et al. [27]. Linear models proved to be inadequate to yield (p-value = 0.0007), SA (p-value = 0.0359), and HHV (borderline fit p-value = 0.0526) due to significant lack of fit. The two-factor interaction (2FI) model showed an inconsistent performance based on a marginally significant improvement of the lack of fit p-value of 0.0135 and 0.0014 for HHV and yield response, respectively, but poorly underperformed for SA response (insignificant sequential p-value = 0.8808 and negative predicted R^2 = −0.0546). Overall, the quadratic model outperformed all the models, showing highly significant sequential p-values (<0.05), adequate lack of fit (>0.05), and adjusted R^2 (0.84–0.96 % generally good), indicating higher order models, adequate fit, and good explanatory power, respectively [28]. Cubic models proved to be problematic, exhibiting aliasing behaviour possibly due to insufficient data and the CCD design employed, which does not support third-order estimation. In comparison, yield response (predicted R^2 = 0.8668) is the most accurately predicted, followed by SA (predicted R^2 = 0.6082) and HHV response (predicted R^2 = 0.5746) using the quadratic model. This is because yield is governed by more direct and consistent mass conservation mechanisms during HTC process. Notably, the SA response exhibited the most drastic improvement, with quadratic models indicating that its development is highly non-linear and driven by complex pore formation and collapse. HHV response showed the most balanced progression through model orders reflecting the multi-faceted nature of energy densification during HTC. This phenomenon can be explained by direct linear effects (temperature-driven carbonisation), interactive effects of temperature and S/L ratio, and curvature effects (optimal FW blending ratios), which collectively govern the complex thermochemical transformations, dehydration, and carbon-oxygen exchange that determine the final energy content of the HC. The consistent, robust performance of quadratic models on the three responses suggests that HTC is a process governed by non-linear relationships and interaction effects between process variables. The quadratic model was the highest order polynomial equation that well described the relationship between the factors and three responses coded Equations (4) and (5)-(6).

$$\text{Yield (\%)} = +36.96 - 8.88A - 0.374B + 2.84C - 8.78D - 1.23AB + 0.7373AC + 0.8152AD - 4.02BC - 1.82BD - 3.02CD + 0.6305A^2 - 2.33B^2 - 3.51C^2 - 1.67D^2 \quad (3)$$

$$\text{Surface area} = +7.68 - 0.9075A + 0.1695B - 0.3296C + 1.77D + 0.3647AB + 0.2831AC - 0.1784AD + 0.3551BC - 0.6541BD - 0.1136CD - 1.61A^2 + 0.4767B^2 - 0.6097C^2 - 0.6712D^2 \quad (4)$$

$$\text{HHV} = +30.91 + 3.93A + 0.3046B + 0.6461C - 1.21D + 0.1758AB + 2.60AC + 1.65AD - 1.92BC - 1.54BD + 0.3639CD - 0.5191A^2 - 1.03B^2 - 0.8837C^2 - 3.10D^2 \quad 5)$$

From the ANOVA analysis (Tables S3–S5), the quadratic models were found to be highly significant (p-value = < 0.0001) with insignificant lack of fit on yield (p-value = 0.0559 and C.V.% = 7.88), SA (p-value = 0.5694 and C.V.% = 17.32), and HHV (p-value = 0.5730 and C.V.% = 8.00) responses, indicating it to be the best fit function of the three responses. Furthermore, the predicted vs. actual plot (Table S6a–S8a) showed that most data points are aligned along the diagonal line, indicating a good model fit, which means the predictions are consistent with

the experimental values [29]. A-temperature, C-S/L ratio, D-BW/PP ratio, BC-time x S/L ratio, BD-time x BW/PP ratio, CD-S/L ratio-BW/PP ratio, B^2, and C^2 were found to be significant factors. In contrast, B, AB, AC, and AD were found to be insignificant factors in the yield response. A-temperature (p-value <0.0001 and F-value = 298.11) was the dominant factor, indicating a strong influence on the yield response. Additionally, B-time alone was found to be insignificant, but significant when interacting with other factors (S/L ratio and BW/PP ratio). The strong curvature effects of B^2 and C^2 indicate non-linear relationships. For the SA response, A, D, BD, and A^2 were found to be significant, but B, C, AB, AC, AD, BC, CD, B^2, and C^2 were not, for HHV response A, D, AC, AD, BC, BD, B^2, C^2, and D^2 were found to be significant, while B, AB, CD, and A^2 insignificant. From the results, A-temperature is most critical for both yield and HHV responses, while it affects SA through quadratic relationships. The D-BW/PP ratio is most critical for SA (pore development), significant for yield (mass conservation), and affects HHV (energy content). Time was found not to be significant for any response, but it showed multiple significant interactions. Depending on the desired HC characteristics, optimal processing varies according to the specific factors. To maximise yield, temperature and the BW/PP ratio are essential; to achieve high SA, the BW/PP ratio and the quadratic effect of temperature should be prioritised; and to attain a high HHV, temperature, along with its interactions with both the S/L and BW/PP ratios, are crucial, verified by perturbation analysis (Table S6b–S8b).

3.2. Interactive effect of factors on the yield response

Fig. 1(a–f) provides an insight into the interactive effects of the parameters on yield during HTC on FW. Fig. 1(a) shows an interactive effect of temperature and time on yield at a constant S/L ratio (1:13) and BW/PP (0.5). The results indicate a significant reduction in HC yield with increasing temperature and time, with the lowest yield (10 %) observed at 260 °C and 180 min, and the highest yield (58 %) at 140 °C and 113 min. This negative correlation was also reported by Periyavaram et al. [17], who noted significant biomass decomposition into volatile compounds due to prolonged reaction times and elevated temperatures, facilitating thermal conversion reactions. A study reported by Nizamuddin et al. [29] demonstrated that an enhanced carbonisation process reduces the retention of solid biomass and consequently lowers yield. Fig. 1(b) shows the interactive effects of S/L ratio and temperature on HC yield. The results reveal that an increase in the S/L ratio, accompanied by a decrease in temperature, enhances HC yield due to increased solubilisation. Similar trend was observed by Ref. [30,31]. It can be explained that a higher S/L ratio enhances the ability of the liquid phase to solubilise biomass-derived compounds for carbon retention, thereby improving HC yield. Conversely, lower S/L ratios tend to reduce HC formation due to a lower liquid phase capacity for carbon retention [32]. Interestingly, a decrease in the BW/PP ratio (0-HC from BW, 1-HC from PP, and 0.5-HC as the mix of BW/PP) led to an increase in yield, as shown in Fig. 1(c), (e), and 1(f). Since, BW is more fibrous with higher lignin-rich as compared to PP, it poses high resistance to hydrolysis under high temperatures [33]. This structural characteristic possibly reduces the conversion efficiency of BW-rich FW. Hence, optimising the BW/PP ratio during the HTC process is essential for improving yield. Fig. 1(d) shows the interactive effects of S/L ratio and time on HC yield. The results reveal that an increase in the S/L ratio, accompanied by a decrease in reaction time, significantly enhances HC yield. This observation is consistent with the results reported by Álvarez-Murillo et al. [30], who demonstrated that the equilibrium between reaction time and the S/L ratio is a crucial factor for maximising HC production, which directly enhances biomass conversion efficiency.

3.3. Interactive effect of factors on the surface area response

As shown in Fig. 3(a)–(c), an increase in temperature up to approximately 220 °C positively influences the SA of HC. This phenomenon may be associated with the development of microporous and mesoporous structures on the carbon matrix resulting from the release of volatile compounds. However, the SA decreased due to pore collapse at temperatures above 220 °C. A similar observation was reported by Saqib et al. [34], where the SA of HC synthesised from FW at 200–300 °C increased and then decreased with increasing operating temperatures. Fig. 2(a, d, and e) highlights the effect of process time on SA. An increase in process time does not significantly affect the SA. This can be attributed to the fact that most structural changes occur once a specific temperature has been reached, hence extending the time has minimal additional effects on SA. Fig. 2(b, d, and f) depicts the impact of the S/L ratio on SA. Increasing the S/L ratio has a minimal effect on the HC SA.

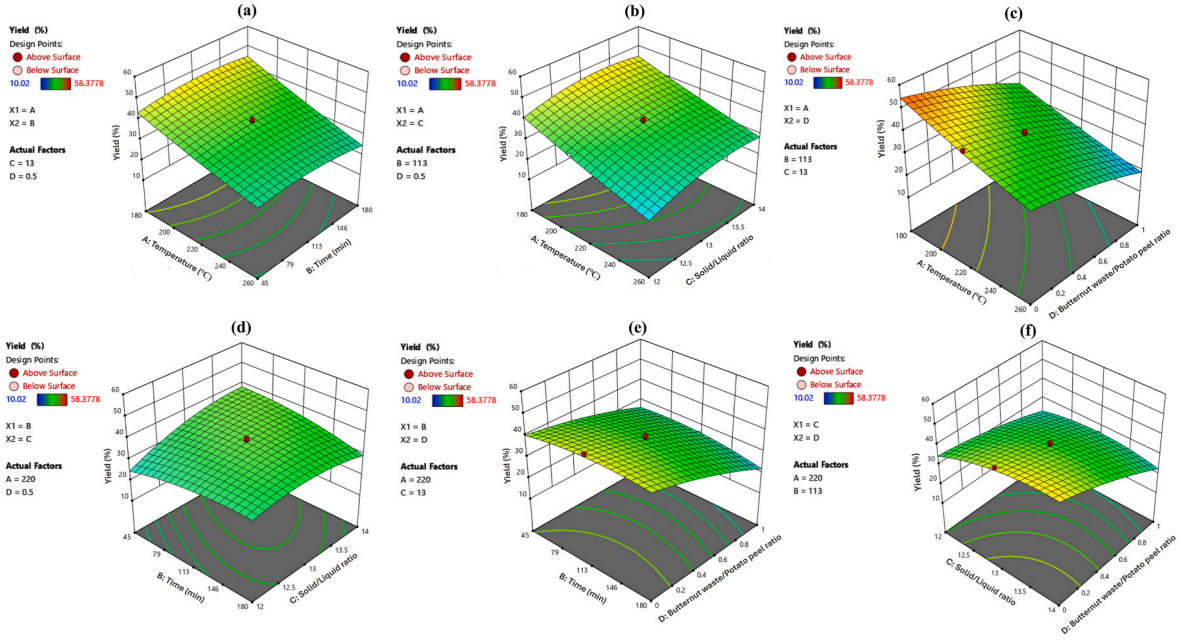

Fig. 1. 3D Response surface for yield showing the effects of (a) temperature and time, (b) temperature and S/L ratio, (c) BW/PP ratio and temperature, (d) S/L ratio and time, (e) BW/PP ratio and time, and (f) BW/PP ratio and S/L ratio.

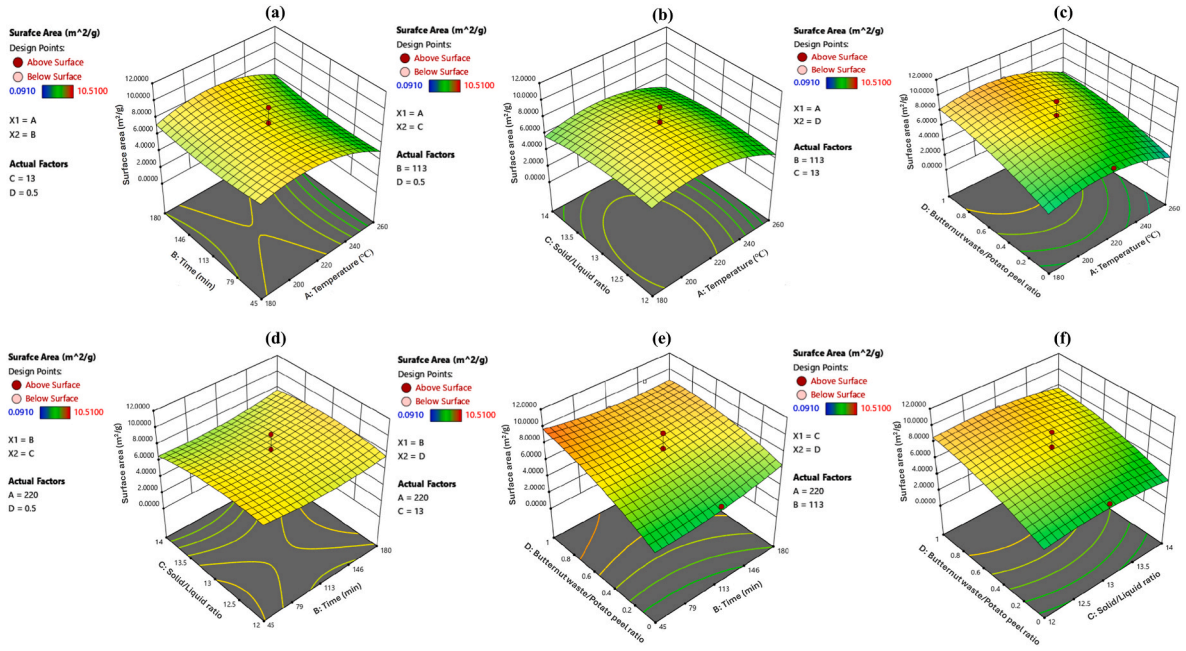

Fig. 2. 3D Response surface for SA showing the effects of (a) temperature and time, (b) temperature and S/L ratio, (c) BW/PP ratio and temperature, (d) S/L ratio and time, (e) BW/PP ratio and time, (f) BW/PP ratio and S/L ratio.

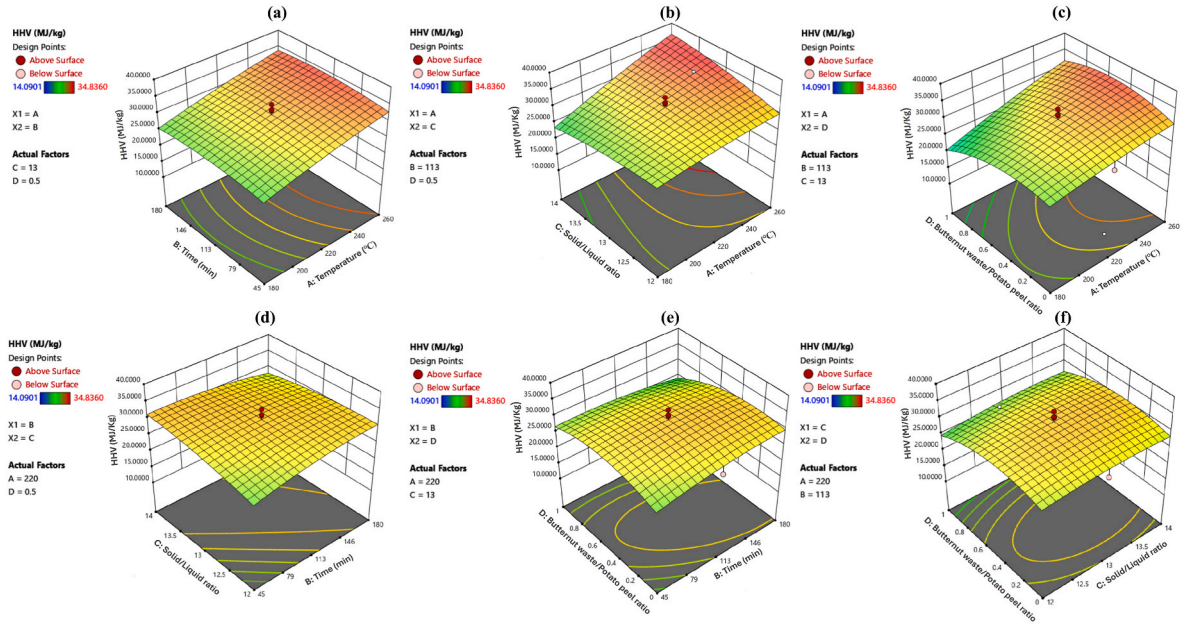

Fig. 3. 3D Response surface for HHV showing the effects of (a) temperature and time, (b) temperature and S/L ratio, (c) BW/PP ratio and temperature, (d) S/L ratio and time, (e) BW/PP ratio and time, (f) BW/PP ratio and S/L ratio.

Since HTC is temperature-dominant, high temperatures may result in the rapid formation of HC, thereby masking the impact of water content. The BW/PP ratio had a significant effect on SA, as evidenced by Fig. 2(c) and (e), and 2 (f). The HC synthesised from PP had a significantly higher SA compared to the HC synthesised from BW. This can be attributed to PP having higher lignin and cellulose content, which facilitates the formation of rigid, porous carbon structures. PP is also more fibrous than the BW, which helps retain the structure and thus improves the porosity of the resultant HC.

3.4. *Interactive effect of factors on the HHV response*

Fig. 3 illustrates the effect of HTC process variables and their interaction on the HHV response. As shown in Fig. 3(a–c), an increase in reaction temperature led to higher HHV, which contrasts with the decreasing trend observed in HC yield. The increase in temperature promotes decarboxylation and dehydration reactions, reducing the O/C and H/C ratios of HC due to carbon enrichment, thereby increasing the HHV [35]. A similar observation was also obtained in a study by Murillo et al. [21] on the valorisation of oat husk by HTC. As demonstrated in Fig. 3(a, d, and e), the effect of HTC residence time was less significant than that of temperature, with the response surface consistently

increasing with increasing temperature. This indicates that residence time contributes only marginally to the increase in HHV compared to the more pronounced impact of reaction temperature. This is because the effect of reaction time on HTC reactions, such as hydrolysis, lasts within a definite time range, and afterwards, no significant change is observed in HHV [36]. Fig. 3(b, d, and f) depicts the influence of the S/L ratio on the HHV. Increasing the S/L ratio had minimal effect on the HHV, as the HHV is an intrinsic property governed by the chemical composition of the solid substrate rather than its concentration in the slurry. A similar trend on the influence of S/L ratio on HHV was also reported by Murillo et al. [21]. The impact of the BW/PP ratio is outlined in Fig. 3(c, e, and f). The BW/PP ratio had a minimum effect on the HHV due to the slight difference in the raw BW and PP in the HHV.

3.4.1. Comparison of the fuel properties of HC-derived FW with other studies

Table 1 presents a comparison of the fuel properties of HC derived from FW in this study with those reported for HC produced from various feedstocks in the literature. In this study, the HHV (27.98 MJ/kg) of FW-derived HC (mixed BW/PP) was obtained at 204 °C, which is markedly higher compared to other studies. For instance, HC derived from rice husk achieved a HHV of 17.60 MJ/kg at 170 °C [37], HC derived from agri-FW achieved a HHV of 24.50 MJ/kg at 300 °C [38], and HC derived from FW achieved a HHV of 21.34 MJ/kg at 150 °C [17]. However, the present study achieved the lowest HC mass yield as compared to the literature [39]. The low mass yield may be due to the increased thermal degradation that occurs at this optimal temperature and prolonged residence time, leading to the conversion of a greater proportion of the organic matter into volatile compounds rather than solid carbonaceous material. The high HHV indicates that the resulting HC is more energy-dense, as it is enriched in carbon content and has a superior energy profile, despite the lower yield. This trade-off highlights the potential for producing high-quality fuel from FW through precise control of HTC parameters, prioritizing energy content over mass yield.

3.5. Optimum conditions for HC preparation

The optimum conditions for HC preparation from FW (BW and PP) were determined based on set constraints (Table S10). The maximum yield (40.22 %), SA (7.86 m^2/g), and HHV (29.351 MJ/kg) were achieved at a temperature of 204 °C, residence time of 131.39 min, S/L ratio of 1:12.89, and BW/PP ratio of 0.5 (1:1) (Table S10). The experiment was conducted under similar optimum conditions to validate the predicted yield, SA, and HHV values, achieving a yield of 36.77 %, SA of 8.42 m^2/g, and HHV of 27.98 MJ/kg. This slight deviation indicates high reproducibility of the quadratic model for the three responses. Importantly, optimisation reveals a trade-off in parameters, indicating the potential to enhance yield and HC characteristics from FW. This can be achieved by precisely controlling HTC conditions to tailor HC characteristics for specific application requirements, prioritizing optimised functionality for adsorption or energy over maximising mass yield.

3.6. Characterisation of food waste and hydrochar samples

3.6.1. Elemental composition

Table 2 presents the ultimate analysis of raw FW and the HC samples at varying operating conditions. Ultimate (elemental) analysis is crucial for evaluating the elemental composition of a material, which plays a vital role in determining the oxygen demand required for efficient biofuel combustion [37]. The results reveal significant trends influenced by HTC process conditions and the composition of the feedstock. The higher nitrogen content in the FW compared to the HC samples can be attributed to the significant amounts of protein-rich materials and other organic matter. In comparison to the raw FW, the HC samples produced at higher reaction severities exhibited significant variations in the CHONS composition, which also aligns with previous research ([23]; . The carbon content in HC samples ranged from 47.38 wt% to 73.07 wt %, with higher values typically obtained at elevated temperatures and longer residence times, indicating enhanced dehydration and decarboxylation, which further contributed to the increased HHV of the HC [40]. The HC hydrogen content varied between 5.27 wt% and 9.53 wt%, generally decreasing with higher operating conditions as volatiles are driven off. The nitrogen content observed in HC samples synthesised for shorter reaction times was higher compared to those synthesised at longer times due to the degradation of fewer proteins. The oxygen content ranges from 5.82 wt% to 41.66 wt% and consistently decreases with increasing temperature and time, thereby improving the energy density of the solid HC [41]. The sulphur content remained low across all the samples (<0.1 wt%), with few exceptions, which is favourable for minimising environmental pollution during utilisation. Overall, higher carbon and lower oxygen contents in samples produced under high-severity conditions suggest suitability for use as solid fuels or carbon-rich materials [40]. The HTC process also led to a reduction in nitrogen and sulphur content, which is advantageous as it lowers the potential emissions of NO_x and SO_x during the combustion of HC as a solid fuel [21].

To further understand the chemical evolution of the FW samples during the HTC process at varying operating conditions, the Van Krevelen diagram was utilised, as seen in Fig. 4. The atomic H/C against O/C provides an insight into the degree of carbonisation and the evolving chemical structure of the material. The H/C and O/C ratios decreased with increasing reaction temperature and time, with the HC product synthesised at 260 °C and 180 min, closer to the sub-bituminous region. This can be attributed to the removal of oxygen from the raw FW

Table 1
Comparison of properties from different optimised HTC processes.

Feedstock	Parameters	Ranges	Optimal Conditions	Response	Optimal Values	Ref
FW	Temperature (°C)	160–260	198.5	M_Y[a]	62.05	[17]
	Time (min)	40–360	150	HHV	21.34	
	S/L (g/g)	0.067–0.2	0.2			
Spent coffee grounds	Temperature (°C)	180–220	216.4	M_Y[a]	63.93	[39]
	Time (min)	60–300	60	HHV	–	
	S/L (g/g)	0.1	–			
Agri-FW	Temperature (°C)	190–230	211.5	M_Y[a]	–	[38]
	Time (mins)	60–300	300	HHV	24.50	
	S/L (g/g)	5–20	7.8			
Rice husk	Temperature (°C)	150–200	170	M_Y[a]	71.80	[37]
	Time (min)	10–30	22	HHV	17.60	
	S/L (g/g)	0.125–0.25	0.222			
FW (BW/PP)	Temperature (°C)	140–300	204	M_Y[a]	36.77	**Current study**
	Time (min)	22–248	131	HHV	27.98	
	S/L (g/g)	11–15	13			

[a] M_Y – Mass yield (wt.%).

Table 2
Elemental composition of raw FW and HC samples under varied conditions.

Sample	Temp (°C)	Time (min)	S/L ratio	BW/PP ratio	Ultimate analysis (wt.%)				
					C	H	N	O	S
BW					50.24	7.06	5.73	29.47	0.28
PP					44.56	6.08	5.39	41.66	0.80
1	260	45	12	1	67.66	5.96	4.22	15.07	0.00
2	180	180	12	0	52.80	5.27	3.28	35.59	0.00
3	220	22	13	0.5	60.33	6.53	3.57	15.82	0.67
4	220	113	13	0.5	64.76	6.37	3.71	21.87	0.00
5	220	113	13	0.5	64.49	6.55	3.91	21.47	0.11
6	300	113	13	0.5	72.54	6.86	4.38	12.09	0.12
7	220	248	13	0.5	63.14	5.79	4.31	22.17	0.04
8	180	45	12	1	50.59	5.79	3.34	35.18	0.03
9	180	180	14	0	56.57	5.67	4.45	29.10	0.08
10	260	45	14	0	71.52	7.44	4.20	14.34	0.07
11	260	180	12	0	72.24	6.21	4.18	13.96	0.06
12	140	113	13	0.5	45.60	6.09	2.84	40.31	0.00
13	220	113	11	0.5	63.47	6.09	3.70	22.69	0.08
14	180	45	12	0	52.84	5.64	3.46	34.22	0.03
15	260	45	14	1	68.64	6.37	4.26	17.12	0.06
16	220	113	15	0.5	63.93	6.42	3.47	22.54	0.06
17	180	45	14	1	54.82	6.19	3.62	30.42	0.08
18	220	113	13	0.5	64.98	6.26	3.75	21.60	0.06
19	260	180	12	1	72.10	6.29	4.18	13.20	0.05
20	220	113	13	1	64.73	5.90	3.51	22.59	0.07
21	260	45	12	0	69.69	7.31	4.10	14.74	0.06
22	260	180	14	1	73.07	6.68	4.11	13.11	0.10
23	220	113	13	0.5	63.08	6.39	4.15	22.42	0.08
24	220	113	13	0.5	62.08	6.11	3.60	24.79	0.09
25	260	180	14	0	70.99	6.84	4.70	13.81	0.00
26	180	180	12	1	54.39	5.76	3.77	31.00	0.06
27	220	113	13	0.5	59.17	5.88	3.77	26.47	0.06
28	180	45	14	0	47.38	5.80	4.12	39.53	0.00
29	180	180	14	1	55.34	5.81	3.59	30.79	0.04
30	220	113	13	0	65.54	6.68	3.84	20.00	0.05

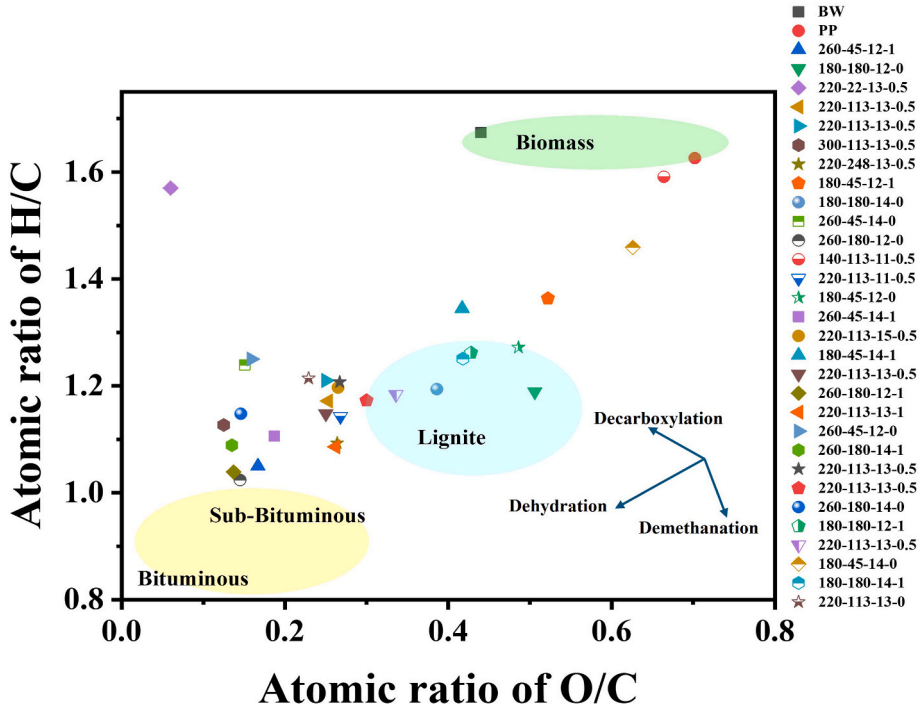

Fig. 4. Van Krevelen diagram of raw FW (BW and PP) and HC samples at varying operating conditions [Numerical sample labels: W-X-Y-Z referred to temperatures-residence time-S/L ratio-BW/PP ratio].

samples during dehydration and decarboxylation reactions, which enhances the carbonisation degree of the HC product [25]. Thus, contributing to the higher HHV of the HC produced.

3.6.2. *Proximate analysis*

Table 3 summarises the proximate analysis results of the raw FW and HC samples synthesised at varying operating conditions. Proximate

Table 3
Proximate analysis of raw FW and HC samples at varying process conditions.

Sample	Temp (°C)	Time (mins)	S/L ratio	BW/PP ratio	Proximate analysis (wt.%)			
					MC	VM	Ash	FC
BW					88.00	75.82	7.50	13.86
PP					78.00	76.89	5.31	15.00
1	260	45	12	1	1.38	55.06	7.09	36.46
2	180	180	12	0	3.09	63.35	3.06	30.51
3	220	22	13	0.5	1.99	71.33	4.75	21.93
4	220	113	13	0.5	2.15	62.85	3.29	31.70
5	220	113	13	0.5	1.61	67.72	3.58	27.10
6	300	113	13	0.5	0.82	60.22	4.13	34.83
7	220	248	13	0.5	2.36	61.04	4.59	32.01
8	180	45	12	1	3.23	72.12	5.10	19.55
9	180	180	14	0	2.35	67.75	4.21	25.69
10	260	45	14	0	0.71	66.52	2.50	30.26
11	260	180	12	0	1.67	52.79	3.41	42.13
12	140	113	13	0.5	1.96	78.78	5.16	14.10
13	220	113	11	0.5	1.78	63.02	4.05	31.15
14	180	45	12	0	2.20	72.20	3.84	21.76
15	260	45	14	1	1.12	57.56	3.61	37.71
16	220	113	15	0.5	1.74	63.96	3.64	30.65
17	180	45	14	1	3.07	70.33	4.95	21.65
18	220	113	13	0.5	1.62	62.19	3.41	32.78
19	260	180	12	1	1.53	52.45	4.23	41.80
20	220	113	13	1	1.82	58.14	3.27	36.77
21	260	45	12	0	0.84	65.14	4.16	29.86
22	260	180	14	1	0.83	57.19	3.03	38.95
23	220	113	13	0.5	1.55	69.13	3.96	25.36
24	220	113	13	0.5	1.59	65.05	3.42	29.95
25	260	180	14	0	0.94	60.37	3.66	35.02
26	180	180	12	1	4.83	66.31	5.08	23.77
27	220	113	13	0.5	1.90	60.44	4.71	32.95
28	180	45	14	0	1.94	73.82	3.17	21.07
29	180	180	14	1	3.38	62.20	4.47	29.95
30	220	113	13	0	2.09	72.68	3.94	21.29

analysis assesses the energy content by analysing the combustible components (VM and FC) and the non-combustible components (MC and ash) of HC as a solid feed [41]. The proximate analysis of the BW and PP shows key differences that influence the properties of the resulting HC. BW exhibited a higher MC of 88.00 wt% compared to PP at 78.00 wt%, while both feedstocks showed relatively similar content of VM (75.82 wt % for BW and 76.89 wt% for PP) and low FC content (13.86 wt% and 15.00 wt%, respectively). The MC is primarily due to the cell vacuoles and interstitial spaces, which are common in fresh produce. High VM is also indicative of the relatively low lignin content typical of vegetative waste compared to woody biomass. Additionally, low FC is due to a greater proportion of cellulose and hemicellulose in BW and PP, which, upon thermal processing, yield more volatiles and fewer stable char residues, thus contributing to low FC. These findings indicate that both feedstocks in their raw state are not ideal fuels due to excessive moisture and low carbon stability. Varying process parameters significantly affected the proximate composition of the HC product. Temperature had the most significant influence.

As the temperature increased, moisture and VM content generally decreased, while FC increased. HC produced at 300 °C had a very low MC (0.82 wt%) and VM (60.22 wt%), while the FC content increased (34.83 wt%). In contrast, HC produced at 140 °C resulted in HC with high VM (78.78 wt%) and low FC (14.10 wt%), indicating the significance of higher temperatures for effective carbonisation. Reaction time also had an influence, particularly at elevated process temperatures. Longer residence times resulted in further decomposition of VM and enhanced the FC content. Increasing the time from 45 min to 180 min at 260 °C resulted in a decrease in VM from 55.06 wt% to 52.79 wt% and an increase in FC from 36.46 wt% to 42.13 wt%. This trend can be attributed to enhanced coalification, decarboxylation, and dehydration reactions occurring at high temperatures and reaction times [42]. Although the impact of time was less pronounced than temperature, it became more significant at higher HTC temperatures. The S/L ratio influenced the thermal environment and mass transfer during HTC. Lower S/L ratios improved dispersion and hydrolysis, resulting in slightly higher FC content [43]. Increasing the S/L ratio from 1:11 to 1:15 at similar operating conditions slightly decreased FC content from 31.15 wt% to 30.65 wt%. The feedstock composition also significantly affected the HC proximate characteristics. The HC sample produced from equal amounts of BW and PP exhibited a high FC content compared to those made from homogeneous feedstocks. This indicated that blending feedstocks influenced hydrochar properties. The results suggest that elevated temperatures and longer residence times favour FC enrichment in HC, while feedstock composition and S/L ratio moderately influence these proximate characteristics. Most of the samples showed reduced ash content compared to the raw BW (7.50 wt%) and raw PP (5.31 wt%), indicating partial removal of inorganics during HTC. Despite being produced under identical HTC conditions, HCs from different feedstocks exhibited different ash content. This could be ascribed to the differences in mineral composition and ash-forming tendencies between BW and PP. Blended feedstocks typically showed ash contents between 3.27 and 4.95 wt%, suggesting a moderate and consistent ash retention behaviour due to the balancing effect between the two biomass types. HC samples processed at longer times and lower S/L ratios generally exhibited lower ash content, likely due to enhanced leaching of soluble minerals. Overall, the results affirm that elevated temperatures and extended residence times enhance FC enrichment in HC, directly correlating with the HHV of the produced HC. These results align with previous studies for the HTC of cellulose [44], olive mill wastes [32], and lignocellulosic biomass [45].

3.6.3. *Surface morphology analysis*

Fig. 5 presents the SEM morphology of raw FW and HC samples prepared under varying conditions at a magnification of ×2000, linking their characterisation to adsorption properties and HHV applications. In Fig. 5(a–b), the morphology of the raw FW samples depicts spherical

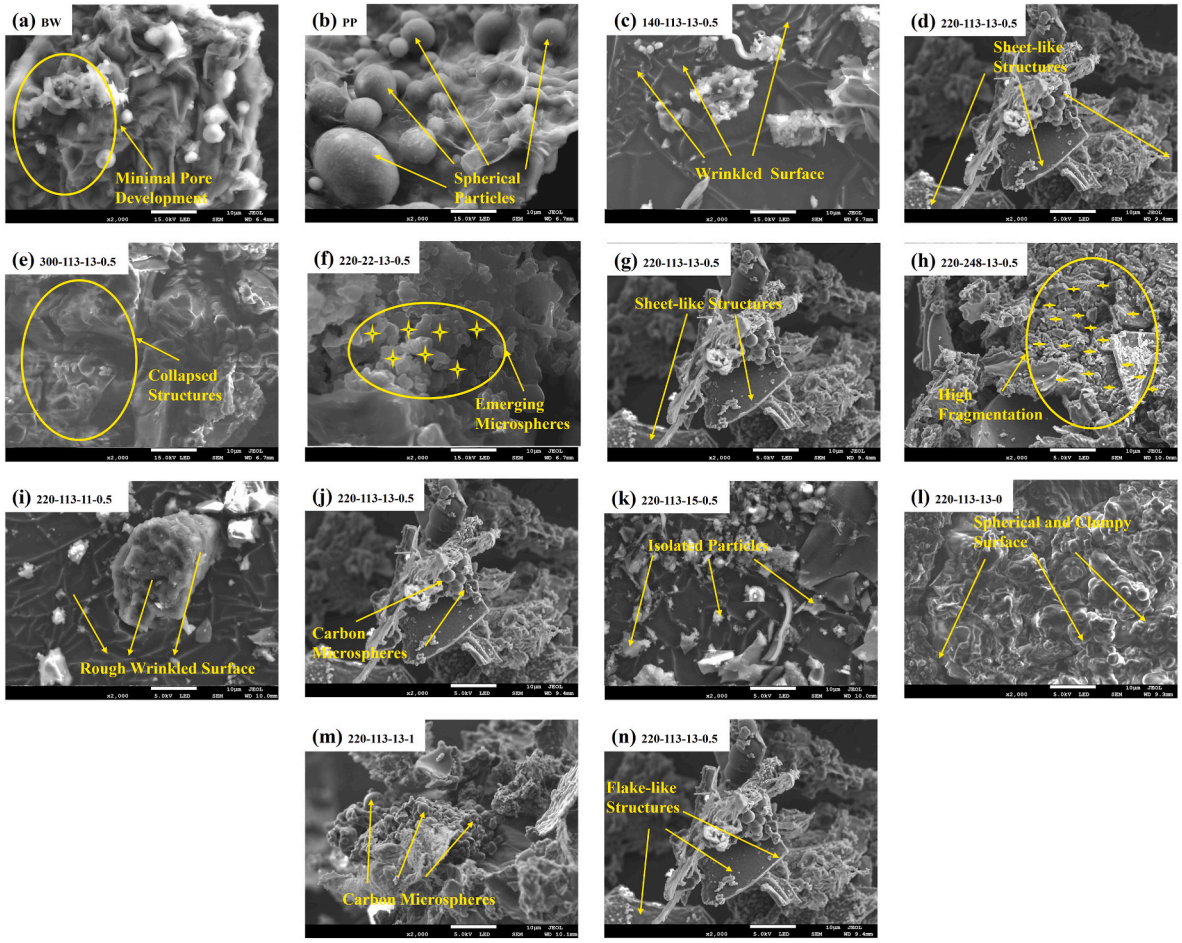

Fig. 5. SEM images comparing raw FW biomass (a–b) to hydrochar produced under different conditions: temperature (c–e), time (f–h), S/L ratio (i–k), and mixed BW/PP (l–n). [Numerical sample labels W-X-Y-Z referred to temperatures-residence time-S/L ratio-BW/PP ratio].

deposits on the biomass surface and minimal pore development. These characteristics can be attributed to the natural biominerals (phytoliths) or structured bump features present in untreated biomass [46]. Similar silica-structured bumps in biomass were also reported by Alhinai et al. [47] during the production of biochar from rice husk. These structured features indicate their potential for pollutant uptake and porous carbon-based biofuel. Fig. 5(c–e) shows the morphology of HC samples at temperatures of 140 °C, 220 °C, and 300 °C, respectively. A wrinkled surface morphology is observed at low temperatures, indicating thermal shrinkage and dehydration. However, at high temperatures, the biomass structure is severely degraded due to intense HTC reactions [48]. The intense HTC can enhance the energy density by modifying the structural properties that impact adsorption capabilities. Fig. 5(f–h) displays the HC micrography at times of 22 min, 113 min, and 248 min, respectively. Microspheres emerge at the lowest residence time, with higher fragmentation observed at increased reaction durations. The emerging microspheres can be attributed to incomplete degradation, as the reaction is intense and short-lived (intermediate stage of HTC) [49]. The observed fragmentation is due to the breakdown of lignin, hemicellulose, and cellulose, leading to structural collapse [50]. By enhancing SA for adsorption and increasing fixed carbon for HHV, this fragmentation directly tailors HHV for dual application in pollutant removal and energy recovery. As highlighted in Fig. 5(i–k), increasing the S/L ratio led to a highly dilute environment, promoting the formation of thin carbon films and smoother carbon microspheres due to enhanced solubilisation and recondensation dynamics [51]. These structural changes contribute to the large SA and carbon densification, which can positively affect the adsorptive properties of HC and improve fuel ratios, respectively. In Fig. 5(l–n), the morphology of HC from the PP, BW, and the heterogeneous mix can be seen. The HC from homogenous feedstocks depicted a more uniform surface texture due to homogenous compositions. PP HC exhibited a dense, spherical, and clumpy surface due to its high starch content. In contrast, the BW HC showed numerous carbon microspheres mainly due to the high fibre content in the feedstocks' cellulose and hemicellulose [52]. The heterogeneous HC sample exhibited flask-like structures due to dehydration and aromatisation (Fiori et al., 2014), which is important for the adsorption of pollutants, as their unique geometry offers high capacity and strong retention.

3.6.4. *Surface functional groups*

FTIR analysis was utilised to examine the changes in surface functional groups of the raw FW samples (rBW and rPP) and the corresponding HC products ($_{HC}$BW-PP$_{x-y}$) obtained at different operating conditions, and the FTIR spectra are shown in Fig. 6. The peak at 3400 cm^{-1} is assigned to the -OH vibrational group, which can be attributed to the hydroxyl group of water in the feedstock sample [19]. The peak at 2800 cm^{-1} is from the C-H group, which shows the presence of aliphatic substances [53]. The wavelength range of 1800 to 700 cm^{-1} corresponds to the characteristic resonance region of oxygen-containing functional groups, primarily including aromatic ring (C=C), carbonyl (C=O), ether linkages (C–O), and the bending vibrations of methyl groups [54].

In Fig. 6(a), the spectra of the raw FW and the HC showed some similarity in shape. Still, the vibrational peaks of the HC prepared at varying temperatures were significantly different. Interestingly, in contrast to previous studies, which reported a progressive decline in the

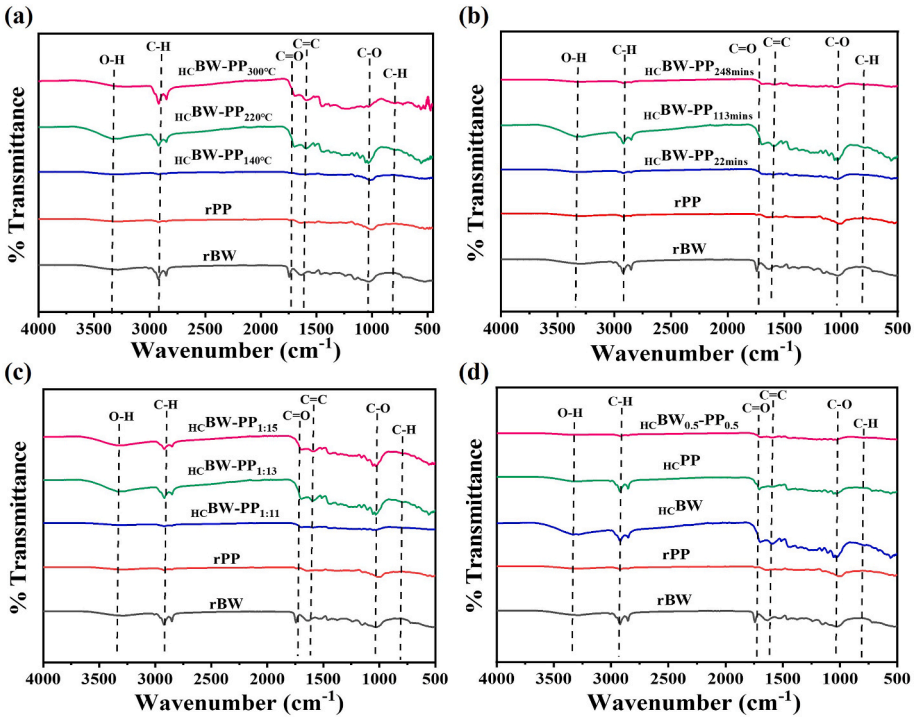

Fig. 6. Fourier transform infrared spectra of raw butternut waste (rBW), raw potato peels (rPP) and synthesised HC ($_{HC}$BW-PP$_{x\text{-}y}$) at varying (a) Temperature, (b) Time (c) S/L ratio (d) Feedstock ratio.

-OH stretching vibration with increasing HTC temperature due to dehydration and the loss of hydroxyl-containing functional groups [25], the present study observed a notable persistence and slight increase of the O-H peak at higher temperatures (220–300 °C). This unusual result may be attributed to the formation of new phenolic -OH groups from lignin-like condensation products, or to surface-bound water re-adsorbed due to the increased porosity of HC. This trend deviates from the expected outcome and suggests that secondary reactions during HTC might reintroduce or stabilise hydroxyl functionalities under certain conditions. The intensity of the C-H peak significantly increased with the increase in HTC temperature, which can be attributed to the repolymerisation of HC into waxier, aliphatic structures. Such findings suggest that secondary reactions during HTC may help retain or stabilise hydroxyl functionalities under specific conditions, thereby enhancing the HC adsorption capacity for pollutants.

In Fig. 6(b), increasing the HTC residence time enhanced carbonisation of the FW samples. This can be evidenced by the reduction of O-H and C-O peaks and the intensification of the C=C band. An increased degree of carbonisation can significantly enhance the carbon densification. These changes suggest progressive dehydration, decarboxylation, and aromatic condensation, consistent with enhanced HC stability and lower polarity at extended reaction times [40]. Increasing the solid-to-water ratio, as shown in Fig. 6(c), resulted in HC with higher oxygenated functional groups, as indicated by the intensified -OH and C=O peaks in the FTIR spectra. This trend suggests milder reaction severity and less extensive aromatisation, likely due to the dilution of reactive intermediates. These findings align with previous studies, which report that high water ratios enhance the preservation of polar surface functionalities, thereby improving the adsorptive properties of the HC [55]. In Fig. 6(d), the observed decrease in the O-H, C=O, C-H, and C-O peaks in the FTIR spectra of HC from the mixed butternut and potato peels feedstock suggests enhanced thermal degradation and transformation of organic functional groups. The blending may have intensified dehydration, decarboxylation, and depolymerisation reactions, resulting in fewer surface hydroxyl, carbonyl, aliphatic, and ether groups [10]. These alterations underline the complex interplay between FW composition and functional group preservation, key factors influencing the adsorption capabilities of HC for pollutant removal.

3.6.5. X-ray diffraction analysis

The XRD patterns of raw FW samples and the corresponding HC products ($_{HC}$BW-PP$_{x\text{-}y}$) obtained at different conditions are illustrated in Fig. 7. The raw BW and PP samples show well-defined peaks at 2θ of 16^0 (001) and 22^0 (002), and this may be ascribed to the lateral arrangement of microcrystals and the linear configuration of polymer chains. [56]. While the HC peak patterns were similar to those of the raw FW samples in Fig. 7(a), variations were evident because of the interplay between lignin and hemicellulose. An increase in HTC process temperature significantly decreased the cellulose peaks, while the lignin peaks became more pronounced. This shift indicated cellulose decomposition into amorphous carbon [57]. Fig. 7(b) shows similar trends with increasing HTC reaction time from 22 to 248 min. Broad peaks at 2θ of 23^0 (15-35^0) and 43^0 (40-45^0), corresponding to (002) and (101) planes respectively, are observed. The (002) and (101) diffraction planes correspond to amorphous and graphitic carbon with low degrees of graphitisation. Fig. 7(c) depicts the impact of the biomass-to-water ratio (BWR) on the resultant HC product. The sharp cellulose peaks diminish as water content increases, suggesting enhanced carbonisation and condensation of lignin and solubilised components [58]. Homogeneous (rBW and rPP) and heterogeneous (mixture) HC samples are illustrated in Fig. 7(d). The homogenous BW HC pattern shows a sharp peak at around 22^0 compared to PP, suggesting a more complete breakdown of the crystalline region in the PP HC. The heterogeneous HC sample shows a broader hump, indicating synergistic HTC reactions.

3.6.6. Thermal decomposition behaviour and thermal characteristics

The weight loss (TG) and the rate of weight loss (DTG) of raw FW samples (rBW and rPP) and their HC products ($_{HC}$BW-PP$_{x\text{-}y}$) synthesised at varying conditions are presented in Figs. 8 and 9, respectively. In Fig. 8(a–d), a small weight loss peak is observed from 50 to 150 °C, which can be attributed to moisture loss [59]. This peak is more prominent in raw FW samples due to high water content. The HC

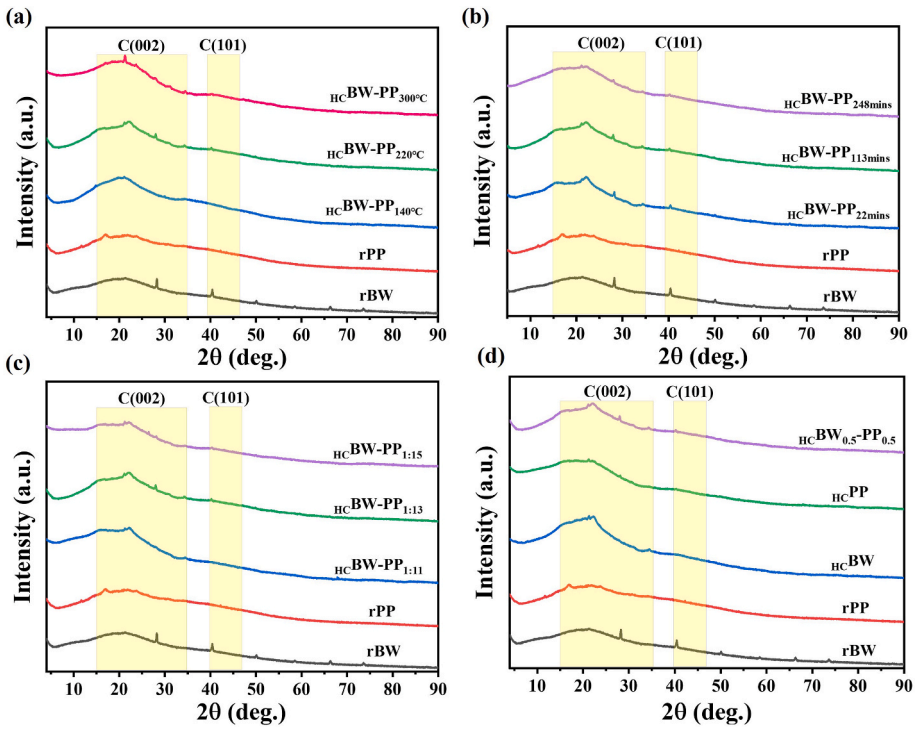

Fig. 7. X-Ray diffraction patterns of raw butternut waste (rBW), raw potato peels (rPP) and synthesised HC ($_{HC}$BW-PP$_{x\text{-}y}$) at varying (a) Temperature (b) Time (c) S/L ratio (d) Feedstock ratio.

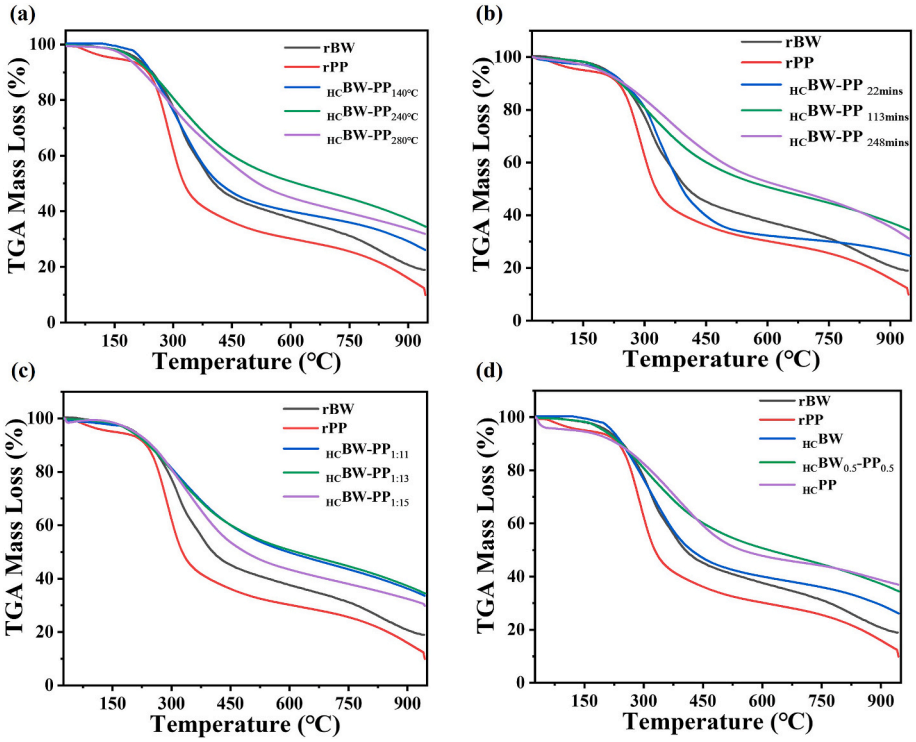

Fig. 8. TGA curves of raw butternut waste (rBW), raw potato peels (rPP) and synthesised HC ($_{HC}$BW-PP$_{x\text{-}y}$) at varying (a) Temperature (b) Time (c) S/L ratio (d) Feedstock ratio.

samples show less weight loss due to prior drying during HTC. Within the temperature range 200–350 °C, a second weight loss peak can be observed. This peak can be attributed to VM released from the samples. The VM consists mainly of devolatilisation products of hemicellulose and cellulose [60]. Between 375 and 900 °C, a third weight loss peak is observed, indicating the decomposition of the organic fraction in the respective samples [61]. This peak is relatively slow and minor due to the decomposition of the inorganic content of biomass, like ash, which is more stable. At high temperatures, the remaining devolatilisation and char decomposition occur. From Fig. 8(a), the TGA of HC produced at

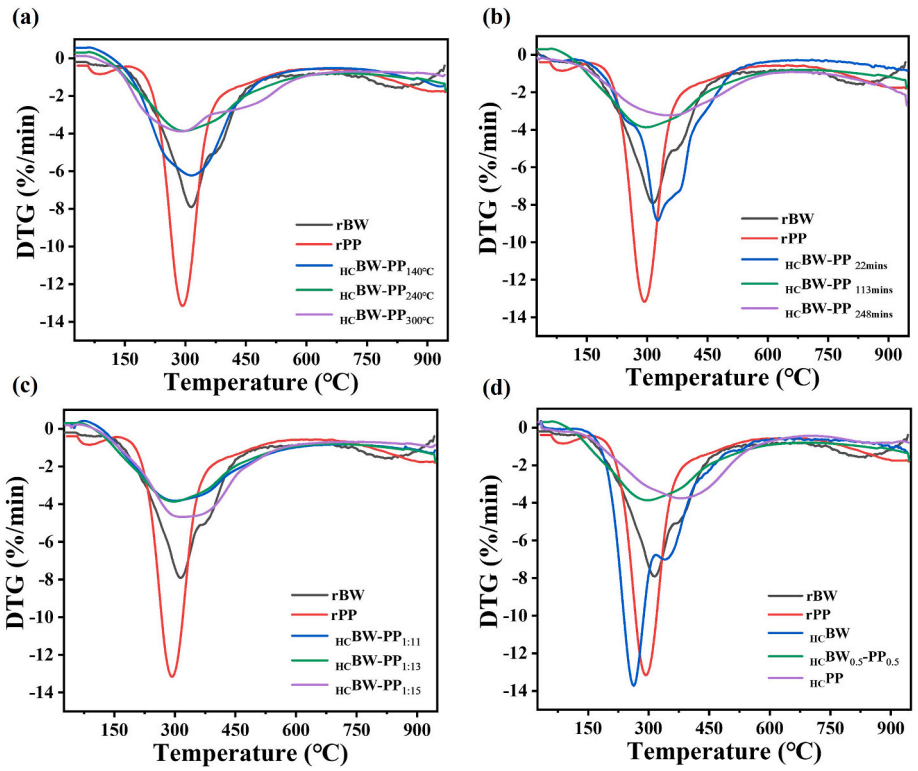

Fig. 9. DTG curves of raw butternut waste (rBW), raw potato peels (rPP), and synthesised HC ($_{HC}$BW-PP$_{x\text{-}y}$) at varying (a) Temperature (b) Time (c) S/L ratio (d) Feedstock ratio.

high HTC temperatures reveals increased thermal stability. Raw biomass exhibits significant mass loss at low temperatures due to its high moisture content and thermally unstable components, such as cellulose and hemicellulose, resulting in a sharp degradation peak between 200 and 350 °C and a low residual mass. In contrast, HC samples show progressively reduced MC and lower volatile decomposition as HTC temperature increases. The weight loss peaks in HC samples become less intense at higher temperatures, indicating improved thermal stability [25]. The HC samples produced at higher temperatures leave more residual mass (FC and ash), indicating greater carbonisation. Increasing the HTC residence time significantly influences the thermal behaviour of the HC samples. As residence time extends from 22 to 248 min, there is greater carbonisation, resulting in increased carbon content, lower O/C and H/C ratios, and a decline in VM. This results in improved thermal stability, as evidenced by Fig. 8(b), where the prominent weight loss peak becomes less pronounced and shifts to higher temperatures, and the residual mass increases in HC synthesised at 248 min [7]. Varying the solid-to-water ratio during HTC significantly influences the properties of the resulting HC as shown in Fig. 8(c). The HC produced at a higher water ratio (1:15) exhibits lower carbon content and thermal stability due to dilution of intermediates and slower secondary polymerisation reactions. In contrast, lower water ratios (1:11) promote more extensive polymerisation and condensation reactions, resulting in HC with greater FC content and higher thermal stability as seen in TGA [62]. Fig. 8(d) shows the effect of varying feedstock ratios. The HC sample, which contained a mixture of PP and BW, resulted in a more stable weight loss profile and increased residual mass compared to the homogeneous samples. This can be attributed to more favourable polymerisation of intermediate compounds during HTC [10].

As depicted in Fig. 9, the DTG curves of the raw FW and the HC samples exhibited three distinct peaks. These peaks were located between 75 and 150 °C, 225–375 °C, and 750–900 °C, respectively. The weight loss peak below 150 °C was assigned to the loss of moisture. The second peak was attributed to oxidation and removal of VMs, leading to char formation, while the third peak was related to char combustion [63]. In the case of raw FW, two peaks (75–150 °C and 225–375 °C) were identified during the combustion process. The DTG curves of the HC samples were seen to separate into two combustion stages (two different peaks) after the moisture removal. The temperature ranges of these two peaks of HC gradually moved towards higher temperature regions. As HTC temperature and time increased, the peak between 750 and 900 °C became more pronounced Figure (a–b). This increase in the third peak may be due to an increase in carbon content [64]. From Fig. 9(c), the HC sample prepared at a S/L ratio of 1:15 had a higher DTG mass loss at lower temperatures, indicating less condensed carbon structure in the solid residue [7]. In Fig. 9(d), the HC sample prepared from BW had a greater mass loss at low temperatures compared to that synthesised from PP and the mix, due to more VM in the BW feedstock.

4. Conclusion

This study successfully investigated the production of HC derived from FW, specifically BW and PP, under varied HTC conditions (temperature, residence time, S/L ratio, and BW/PP ratio). RSM-CCD optimised and established the significance of critical HTC factors on multi-response, mainly HC yield and its physicochemical properties (HHV and SA). The optimum conditions to achieve maximum yield (40.22 %), SA (7.86 m^2/g), and HHV (29.351 MJ/kg) were found to be at a temperature of 204 °C, residence time of 131.39 min, S/L ratio of 1:12.89, and BW/PP ratio of 0.5 (1:1). From the results, temperature had the most significant effect on yield HC characteristics. Specifically, the highest HC yield (58.38 %) was achieved at 140 °C, followed by a drastic drop to 20.70 % at 300 °C, mainly due to increased organic matter decomposition. Conversely, HHV reached 34.21 MJ/kg at 300 °C, signifying an enhancement in energy density correlated with increased dehydration and decarboxylation. Additionally, the SA of HC peaked 220 °C (9.76 m^2/g) but decreased to 0.43 m^2/g at 300 °C signifying pore collapse and tar condensation. Further analysis demonstrated that

increasing the S/L ratio from 1:11 to 1:15 improved yield (from 19.98 % to 26.00 %) and HHV (from 26.22 to 27.57 MJ/kg), although it had a minor negative impact on SA. The blending of feedstocks also proved beneficial, with a 1:1 BW/PP mixture producing the highest HHV and SA, suggesting that synergistic interactions enhance HC properties. Proximate and elemental analyses confirmed that elevated temperatures and longer reaction times resulted in improved carbonisation, as reflected in reduced volatile matter and increased fixed carbon content. Characterisation methods, including FTIR, SEM, XRD, and TGA/DTG, confirmed that optimal HTC conditions improve HC quality by increasing aromaticity, porosity, and thermal stability. In conclusion, this study offers valuable insights into optimising the production of hydrogen from food waste, highlighting its potential for sustainable applications in renewable energy, adsorption, and carbon sequestration. Through effective and sustainable valorisation, this study offers a paradigm shift in FW management and the advancement of circular economy practices.

CRediT authorship contribution statement

Danai Pasipanodya: Writing – original draft, Visualization, Validation, Methodology, Investigation, Formal analysis. **Naadhira Seedat:** Writing – review & editing, Visualization, Validation, Supervision, Project administration, Funding acquisition, Conceptualization. **Bilal Patel:** Writing – review & editing, Supervision, Conceptualization. **Rishen Roopchund:** Writing – review & editing.

Declaration of competing interest

The authors declare the following financial interests/personal relationships which may be considered as potential competing interests: Naadhira Seedat reports financial support was provided by National Research Foundation of South Africa. If there are other authors, they declare that they have no known competing financial interests or personal relationships that could have appeared to influence the work reported in this paper.

Acknowledgements

The authors gratefully acknowledge the University of Johannesburg for providing the laboratory facilities, resources, and a supportive research environment that enabled the successful execution of this study. The financial support received from the National Research Foundation (NRF) of South Africa through the Thuthuka Fund (Grant number: TTK220328992) is sincerely appreciated. This funding was instrumental in facilitating the procurement of materials and analytical services necessary for the project. The authors also thank the technical staff and postgraduate support teams within the Department of Chemical Engineering for their assistance during the experimental and characterisation phases.

Appendix A. Supplementary data

Supplementary data to this article can be found online at https://doi.org/10.1016/j.biombioe.2025.108879.

Data availability

Data will be made available on request.

References

[1] Y. Jia, H. Li, X. He, P. Li, Z. Wang, Effect of biochar from municipal solid waste on mechanical and freeze–thaw properties of concrete, Constr. Build. Mater. 368 (2023) 130374.
[2] Statssa, Mbalo brief the missing piece of the puzzel (Issue 09/2023), STATSSA, 2023, pp. 1–8. Available[Online]: (Accessed May 2024).
[3] P.A. Specification, Specification for the assessment of the life cycle greenhouse gas emissions of goods and services, Bsi Br. Stand 978 (2008) 580.
[4] R.N. Salas, J. Miller, M. Neira, Health at COP26: Just the Beginning, British Medical Journal Publishing Group, 2021.
[5] T.P.T. Pham, R. Kaushik, G.K. Parshetti, R. Mahmood, R. Balasubramanian, Food waste-to-energy conversion technologies: current status and future directions, Waste Manag. 38 (2015) 399–408.
[6] H. Bhakta Sharma, S. Panigrahi, B.K. Dubey, Food waste hydrothermal carbonization: study on the effects of reaction severities, pelletization and framework development using approaches of the circular economy, Bioresour. Technol. 333 (2021) 125187.
[7] M.T. Reza, C. Coronella, K.M. Holtman, D. Franqui-Villanueva, S.R. Poulson, Hydrothermal carbonization of autoclaved municipal solid waste pulp and anaerobically treated pulp digestate, ACS Sustain. Chem. Eng. 4 (2016) 3649–3658.
[8] P. Zhao, Y. Shen, S. Ge, Z. Chen, K. Yoshikawa, Clean solid biofuel production from high moisture content waste biomass employing hydrothermal treatment, Appl. Energy 131 (2014) 345–367.
[9] M. Sevilla, A.B. Fuertes, Chemical and structural properties of carbonaceous products obtained by hydrothermal carbonization of saccharides, Chem.–Eur. J. 15 (2009) 4195–4203.
[10] A. Funke, F. Ziegler, Hydrothermal carbonization of biomass: a summary and discussion of chemical mechanisms for process engineering, Biofuel Bioprod. Biorefining 4 (2010) 160–177.
[11] G. Mannarino, A. Sarrion, E. Diaz, R. Gori, M.A. De La Rubia, A.F. Mohedano, Improved energy recovery from food waste through hydrothermal carbonization and anaerobic digestion, Waste Manag. 142 (2022) 9–18.
[12] M.A. Islam, M.S.H. Limon, M. Romić, M.A. Islam, Hydrochar-based soil amendments for agriculture: a review of recent progress, Arabian J. Geosci. 14 (2021) 102.
[13] B. González, J.J. Manyà, Activated olive mill waste-based hydrochars as selective adsorbents for CO2 capture under postcombustion conditions, Chem. Eng. Process. Process Intensif. 149 (2020) 107830.
[14] D. Pasipanodya, N. Seedat, B. Patel, R. Roopchund, Production of hydrochar from the hydrothermal carbonisation of food waste feedstock for use as an adsorbent in removal of heavy metals from water, Biomass Convers. Biorefinery (2024) 1–15.
[15] S. Masoumi, V.B. Borugadda, S. Nanda, A.K. Dalai, Hydrochar: a review on its production technologies and applications, Catalysts 11 (2021) 939.
[16] F. El Ouadrhiri, E.a.M. Saleh, K. Husain, A. Adachi, A. Hmamou, I. Hassan, M. M. Moharam, A. Lahkimi, Acid assisted-hydrothermal carbonization of solid waste from essential oils industry: optimization using I-optimal experimental design and removal dye application, Arab. J. Chem. 16 (2023) 104872.
[17] S.R. Periyavaram, K. Bella, L. Uppala, P.H.P. Reddy, Hydrothermal carbonization of food waste: process parameters optimization and biomethane potential evaluation of process water, J. Environ. Manag. 347 (2023) 119132.
[18] C. Cheng, Q. Guo, L. Ding, A. Raheem, Q. He, S.S. Lam, G. Yu, Upgradation of coconut waste shell to value-added hydrochar via hydrothermal carbonization: parametric optimization using response surface methodology, Appl. Energy 327 (2022) 120136.
[19] K. Kang, S. Nanda, G. Sun, L. Qiu, Y. Gu, T. Zhang, M. Zhu, R. Sun, Microwave-assisted hydrothermal carbonization of corn stalk for solid biofuel production: optimization of process parameters and characterization of hydrochar, Energy 186 (2019) 115795.
[20] M.F. Zulkornain, S. Normanbhay, J.M. Saad, M.F.M.A. Zamri, Optimization of rice husk hydrochar via microwave-assisted hydrothermal carbonization: fuel properties and combustion kinetics, Bioresour. Technol. Rep. 17 (2022) 100888.
[21] H.A. Murillo, J. Pagés-Díaz, L.A. Díaz-Robles, F. Vallejo, C. Huiliñir, Valorization of oat husk by hydrothermal carbonization: optimization of process parameters and anaerobic digestion of spent liquors, Bioresour. Technol. 343 (2022) 126112.
[22] Y. Lin, X. Ma, X. Peng, S. Hu, Z. Yu, S. Fang, Effect of hydrothermal carbonization temperature on combustion behavior of hydrochar fuel from paper sludge, Appl. Therm. Eng. 91 (2015) 574–582.
[23] E.I. Assis, B. Gidudu, E.M. Chirwa, Hydrothermal carbonisation of paper sludge: effect of process conditions on hydrochar fuel characteristics and energy recycling efficiency, J. Clean. Prod. 373 (2022) 133775.
[24] S. Wu, Q. Wang, D. Cui, D. Wu, J. Bai, H. Qin, F. Xu, Z. Wang, Insights into the chemical structure evolution and carbonisation mechanism of biomass during hydrothermal treatment, J. Energy Inst. 108 (2023) 101257.
[25] S. Wu, Q. Wang, D. Cui, X. Wang, D. Wu, J. Bai, F. Xu, Z. Wang, J. Zhang, Analysis of fuel properties of hydrochar derived from food waste and biomass: evaluating varied mixing techniques pre/post-hydrothermal carbonization, J. Clean. Prod. 430 (2023) 139660.
[26] B. Orero, T. Lekgoba, M. Mabuza, J. Elisadiki, T. Sithole, F. Ntuli, T. Mashifana, Insight into hybridization of iron scrap derived Fe3O4 on TiO2: facile synthesis of an eco-friendly photocatalyst, characterization, and photoelectric properties, Results Eng. 27 (2025) 106559.
[27] B. Orero, F. Ntuli, C. Zvinowanda, T. Sithole, T. Mashifana, Sustainable synthesis of activated carbon from water hyacinth via one-step carbonization-H3PO4 activation: optimization and modeling via RSM-artificial intelligence approach, Next Mater. 9 (2025) 101140.
[28] D. Bulanga, B. Orero, S. Sibiya, T. Paepae, T. Mashifana, Water hyacinth-derived adsorbent for removal of diclofenac sodium from aqueous solution: modeling and optimization via RSM-ANN/ANFIS hybrid, Next Mater. 9 (2025) 100997.
[29] S. Nizamuddin, N.M. Mubarak, M. Tiripathi, N.S. Jayakumar, J.N. Sahu, P. Ganesan, Chemical, dielectric and structural characterization of optimized

hydrochar produced from hydrothermal carbonization of palm shell, Fuel 163 (2016) 88–97.
[30] A. Álvarez-Murillo, S. Román, B. Ledesma, E. Sabio, Study of variables in energy densification of olive stone by hydrothermal carbonization, J. Anal. Appl. Pyrolysis 113 (2015) 307–314.
[31] A.S.E. Yay, B. Birinci, S. Açıkalın, K. Yay, Hydrothermal carbonization of olive pomace and determining the environmental impacts of post-process products, J. Clean. Prod. 315 (2021) 128087.
[32] M. Volpe, L. Fiori, From olive waste to solid biofuel through hydrothermal carbonisation: the role of temperature and solid load on secondary char formation and hydrochar energy properties, J. Anal. Appl. Pyrolysis 124 (2017) 63–72.
[33] X. Men, S.-I. Choi, X. Han, H.-Y. Kwon, G.-W. Jang, Y.-E. Choi, S.-M. Park, O.-H. Lee, Physicochemical, nutritional and functional properties of Cucurbita moschata, Food Sci. Biotechnol. 30 (2021) 171–183.
[34] N.U. Saqib, S. Baroutian, A.K. Sarmah, Physicochemical, structural and combustion characterization of food waste hydrochar obtained by hydrothermal carbonization, Bioresour. Technol. 266 (2018) 357–363.
[35] S. Kannan, Y. Gariepy, G.S.V. Raghavan, Optimization and characterization of hydrochar produced from microwave hydrothermal carbonization of fish waste, Waste Manag. 65 (2017) 159–168.
[36] S. Nizamuddin, H.A. Baloch, G.J. Griffin, N.M. Mubarak, A.W. Bhutto, R. Abro, S. A. Mazari, B.S. Ali, An overview of effect of process parameters on hydrothermal carbonization of biomass, Renew. Sustain. Energy Rev. 73 (2017) 1289–1299.
[37] M.F. Zulkornain, A.H. Shamsuddin, S. Normanbhay, J. Md Saad, M.F.M. Ahmad Zamri, Optimization of rice husk hydrochar via microwave-assisted hydrothermal carbonization: fuel properties and combustion kinetics, Bioresour. Technol. Rep. 17 (2022) 100888.
[38] F.O. Kassim, M. Sohail, B. Taylor, O.O. Afolabi, Hydrothermal carbonisation of mixed agri-food waste: process optimisation and mechanistic evaluation of hydrochar inorganic chemistry, Biomass Bioenergy 180 (2024) 107027.
[39] O.O. Afolabi, M. Sohail, Y.-L. Cheng, Optimisation and characterisation of hydrochar production from spent coffee grounds by hydrothermal carbonisation, Renew. Energy 147 (2020) 1380–1391.
[40] C. He, A. Giannis, J.-Y. Wang, Conversion of sewage sludge to clean solid fuel using hydrothermal carbonization: hydrochar fuel characteristics and combustion behavior, Appl. Energy 111 (2013) 257–266.
[41] S.Z. Roslan, M.M. Zainol, K. Bikane, S.S.A. Syed-Hassan, Hydrothermal carbonization of sewage sludge for hydrochar production: optimization of operating conditions using Box-Behnken design coupled with response surface methodology, Biomass Convers. Biorefinery (2024) 1–17.
[42] M.A. Abdoli, R. Ghasemzadeh, Evaluation and optimization of hydrothermal carbonization condition for hydrochar and methane yield from anaerobic digestion of organic fraction of municipal solid waste (OFMSW), Fuel 355 (2024) 129531.
[43] K. Mcgaughy, M.T. Reza, Recovery of macro and micro-nutrients by hydrothermal carbonization of septage, J. Agric. Food Chem. 66 (2018) 1854–1862.
[44] N. Saha, A. Saba, M.T. Reza, Effect of hydrothermal carbonization temperature on pH, dissociation constants, and acidic functional groups on hydrochar from cellulose and wood, J. Anal. Appl. Pyrolysis 137 (2019) 138–145.
[45] S.K. Hoekman, A. Broch, C. Robbins, B. Zielinska, L. Felix, Hydrothermal carbonization (HTC) of selected woody and herbaceous biomass feedstocks, Biomass Convers. Biorefinery 3 (2013) 113–126.
[46] H. Mukhtar, N. Ullah, M. Younas, N. Feroze, N. Ali, A. Fatehizadeh, M. Rezakazemi, Torrefaction interpretation through morphological and chemical transformations of agro-waste to porous carbon-based biofuel, Ecotoxicol. Environ. Saf. 264 (2023) 115426.
[47] M. Alhinai, A.K. Azad, M.A. Bakar, N. Phusunti, Characterisation and thermochemical conversion of rice husk for biochar production, Int. J. Renew. Energy Resour. 8 (2018) 1648–1656.
[48] W.-H. Chen, W.-Y. Cheng, K.-M. Lu, Y.-P. Huang, An evaluation on improvement of pulverized biomass property for solid fuel through torrefaction, Appl. Energy 88 (2011) 3636–3644.
[49] K. Fakkaew, T. Koottatep, C. Polprasert, Effects of hydrolysis and carbonization reactions on hydrochar production, Bioresour. Technol. 192 (2015) 328–334.
[50] Y.W. Chua, H. Wu, Y. Yu, Effect of cellulose–lignin interactions on char structural changes during fast pyrolysis at 100–350 °C, Proc. Combust. Inst. 38 (2021) 3977–3986.
[51] H. Si, C. Zhao, B. Wang, X. Liang, M. Gao, Z. Jiang, H. Yu, Y. Yang, Z. Gu, K. Ogino, Liquid-solid ratio during hydrothermal carbonization affects hydrochar application potential in soil: based on characteristics comparison and economic benefit analysis, J. Environ. Manag. 335 (2023) 117567.
[52] M.E. Mahmoud, G.M. El Zokm, A.E. Farag, M.S. Abdelwahab, Assessment of heat-inactivated marine Aspergillus flavus as a novel biosorbent for removal of Cd (II), Hg (II), and Pb (II) from water, Environ. Sci. Pollut. Control Ser. 24 (2017) 18218–18228.
[53] Y. Zhu, Y. Si, X. Wang, W. Zhang, J. Shao, H. Yang, H. Chen, Characterization of hydrochar pellets from hydrothermal carbonization of agricultural residues, Energy Fuels 32 (2018) 11538–11546.
[54] L. Zhang, Q. Wang, F. Xu, Z. Wang, G. Zhang, Insights into the evolution of chemical structures in hydrochars from hydrothermal carbonization of PVC, J. Energy Inst. 105 (2022) 323–333.
[55] J.A. Libra, K.S. Ro, C. Kammann, A. Funke, N.D. Berge, Y. Neubauer, M.-M. Titirici, C. Fühner, O. Bens, J. Kern, K.-H. Emmerich, Hydrothermal carbonization of biomass residuals: a comparative review of the chemistry, processes and applications of wet and dry pyrolysis, Biofuels 2 (2011) 71–106.
[56] S. Yu, X. Yang, Q. Li, Y. Zhang, H. Zhou, Breaking the temperature limit of hydrothermal carbonization of lignocellulosic biomass by decoupling temperature and pressure, Green Energy Environ. 8 (2023) 1216–1227.
[57] S. Yu, X. Dong, P. Zhao, Z. Luo, Z. Sun, X. Yang, Q. Li, L. Wang, Y. Zhang, H. Zhou, Decoupled temperature and pressure hydrothermal synthesis of carbon sub-micron spheres from cellulose, Nat. Commun. 13 (2022) 3616.
[58] A. Akbari, S.J. Peighambardoust, M. Lotfi, Hydrochar derived from Liquorice root pulp utilizing catalytic/non-catalytic hydrothermal carbonization: RSM optimization and cationic dye adsorption assessment, J. Water Proc. Eng. 55 (2023) 104099.
[59] Z. Yao, X. Ma, Y. Lin, Effects of hydrothermal treatment temperature and residence time on characteristics and combustion behaviors of green waste, Appl. Therm. Eng. 104 (2016) 678–686.
[60] W. Liang, G. Wang, R. Xu, X. Ning, J. Zhang, X. Guo, L. Ye, J. Li, C. Jiang, P. Wang, Hydrothermal carbonization of forest waste into solid fuel: mechanism and combustion behavior, Energy 246 (2022) 123343.
[61] G.K. Parshetti, Z. Liu, A. Jain, M.P. Srinivasan, R. Balasubramanian, Hydrothermal carbonization of sewage sludge for energy production with coal, Fuel 111 (2013) 201–210.
[62] M.T. Munir, N.U. Saqib, B. Li, M. Naqvi, Food waste hydrochar: an alternate clean fuel for steel industry, Fuel 346 (2023) 128395.
[63] A.T. Tag, G. Duman, J. Yanik, Influences of feedstock type and process variables on hydrochar properties, Bioresour. Technol. 250 (2018) 337–344.
[64] A.L. Pauline, K. Joseph, Hydrothermal carbonization of organic wastes to carbonaceous solid fuel–A review of mechanisms and process parameters, Fuel 279 (2020) 118472.